Coherent transient effects due to phase modulation of recoilless γ radiation

E. Ikonen, P. Helistö, T. Katila, and K. Riski*
Department of Technical Physics, Helsinki University of Technology, SF-02150 Espoo 15, Finland
(Received 31 January 1985)

Coherent transient effects due to phase modulation of recoilless γ radiation are considered both theoretically and experimentally. Transients are observed in transmission experiments when the incident radiation field interferes with the induced polarization of the Mössbauer absorber. The transient effects studied in this work resemble those observed in NMR and laser spectroscopy. They offer several new features for Mössbauer measurements. A theory for the time dependence of the recoilless radiation is derived semiclassically with use of a density-matrix formalism. Transient effects in scattering geometry are also briefly commented upon. The theory is applied to several cases of experimental interest. Time-dependent distortions affecting the line shape in conventional Mössbauer measurements are considered, e.g., the transmission minimum is delayed approximately for the lifetime of the excited nuclear state. The time dependence of the oscillatory transient excited by a rapid sweep through the resonance is derived. Transient experiments with sinusoidal phase modulation allow metrological calibration of mechanical displacements. The separation between adjacent zeros of the interference oscillations corresponds to a displacement of the source by half a wavelength of the γ radiation. As compared with conventional Mössbauer measurements, more efficient separation of the source and absorber parameters can be achieved in transient experiments. In addition, the linewidths and line positions are obtained in terms of the modulation frequency which simplifies the calibration of the energy scale. If the phase of the incident radiation is rapidly switched, a simultaneous change is observed in the transmission intensity. An exact expansion shows that, with a thick absorber and an appropriate center shift between the source and absorber line positions, this intensity change can be as large as eight times the maximum conventional resonance absorption. Distortions due to nonideal phase modulation are considered as well. Most measurements were performed with use of the 93-keV Mössbauer resonance of ^{67}Zn in ZnO. Comparative results are also presented from ^{57}Fe experiments with sinusoidal phase modulation. In transient experiments with ^{67}Zn, mechanical displacements of the order of 10^{-13} m were resolved. As a further application the recoilless fractions of both the ^{67}Ga:*ZnO* source (f_s) and of the enriched ^{67}ZnO powder absorber (f_a) were determined and found to be equal: $f_s=0.0212(16)$ and $f_a=0.0213(18)$. In phase-switching experiments, filtering of the driving voltage was used to prevent excitation of mechanical resonances of the piezoelectric drive. With a relatively thick absorber and zero center shift, the observed change in the transmitted intensity was three times the conventional resonance absorption. Good agreement between the theoretical calculations and the experimental data was found.

I. INTRODUCTION

Coherent transient effects due to phase modulation of recoilless γ radiation were first reported by Helistö *et al.*[1,2] The transients can be understood as a coherent response of the resonant absorber nuclei when irradiated with nearly monochromatic (recoilless) phase-modulated γ radiation. In transmission experiments the incident radiation field interferes with the field due to the induced polarization of the absorber nuclei. Oscillatory transients are observed when sinusoidal phase modulation is used at frequencies close to the width of the resonance line.[1] Valuable data about Mössbauer parameters are obtainable from this kind of transient experiment. Another type of transient can be generated with stepwise phase modulation. When the phase of the incident radiation is rapidly switched, the resulting change in the transmitted intensity may largely exceed the conventional resonance absorption.[2]

Transient Mössbauer (TM) experiments have been performed mainly using the Mössbauer resonance of ^{67}Zn in ZnO.[1-4] The enhanced transmission has also been measured using the 14-keV Mössbauer resonance of ^{57}Fe.[2,5] The transients can be observed only during a time comparable to the lifetime of the excited nuclear state. Because the 93-keV state of ^{67}Zn has the longest lifetime of the presently applicable Mössbauer states, it is experimentally most feasible for TM measurements.

The phenomena observed in transient experiments differ from those observed both in conventional Mössbauer measurements and in the quantum-beat[6] measurements. Because of the low modulation frequency no transient effects appear in conventional measurements, whereas in quantum-beat experiments at frequencies substantially higher than the width of the resonance line only steady-state oscillations appear. The formalism of Monahan and Perlow,[7] originally developed for the interpretation of quantum-beat measurements, has turned out

to be useful also in computer analysis of some TM experiments.[1] Quantum-beat experiments have been performed with isotopes ^{57}Fe, ^{67}Zn, and ^{129}I.[1,3,6–10] Due to experimental difficulties the quantum-beat curves measured with ^{57}Fe and ^{129}I have so far contained only small contributions of harmonics higher than the second one. This is in contrast to ^{67}Zn measurements, where more complicated shapes of the transmission curves can be resolved even in the quantum-beat experiments.

Coherent transient effects are a relatively new subject in Mössbauer spectroscopy, but they have well-known analogies in other resonance phenomena. In NMR, the interference between the rf input and the nuclear induction signal causes damped oscillations (wiggles), when the resonance is passed rapidly.[11] Theoretical results[12] based on Bloch equations[13] are in agreement with the measured signals. The wiggles are decaying with a time constant T_2^* corresponding to the effective spin-spin relaxation time. When the modulation frequency is increased above the linewidth of the resonance, the transients do not have time to decay and only steady-state oscillations remain.[14,15] These oscillations are analogous to the above-mentioned quantum beats in Mössbauer spectroscopy. The wiggles are closely related to the free-induction decay (FID) observed with pulse excitation.[16] Both are caused by the decay of the nuclear induction signal. In the wiggles the presence of the rf field causes interference oscillations, whereas in the pulse FID only the nuclear induction signal is observed. Other important transient effects studied in NMR are nutation oscillations[17] and spin echoes,[18] whose observation requires strong exciting fields capable of saturating the polarization in the sample.

The NMR results can be generalized to other noninteracting two-level systems.[19] A novel feature of coherent transients was observed using phase switching of an exciting laser field.[20–22] Fast linear transients[21] with optically thick absorbing media are most similar to phase-switching transients observed in Mössbauer experiments. Also FID,[23,24] photon nutation,[25,26] and photon echo[26,27] have been measured in laser spectroscopy. A notable difference between the NMR and laser transients is caused by (Doppler) broadening of atomic transitions. The main application of coherent transient effects in NMR and laser spectroscopy has been the determination of various relaxation times.

We present here a comprehensive study of coherent transient effects in Mössbauer spectroscopy. A derivation of the transmission intensity of recoilless phase-modulated γ radiation is presented in Sec. II. A classical model is applied to the radiation of the Mössbauer source, and density-matrix formalism is used in the description of the absorber nuclei. The results are in agreement with quantum-mechanical considerations. In Sec. III the theory is applied to phase modulation in different experimental regions. Evaluation of the linewidths and recoilless fractions of both the source and absorber resonances is shown to be possible from a single TM transmission curve. The time dependence of the transmission intensity is calculated for phase-switching experiments. Some effects of nonideal phase modulation are considered. The experimental setup is described in Sec. IV. The piezoelectric transducers used for the modulation of the γ radiation are considered in detail. Experimental results with sinusoidal and stepwise phase modulation are presented and discussed in Sec. V. Transient Mössbauer experiments are applied to the determination of the recoilless fractions of the ZnO source and absorber. Results from phase-switching experiments performed with a thick resonance absorber are presented. The main results are summarized in Sec. VI. In the Appendix, line broadenings are considered by assuming a distribution of resonance frequencies, and a series expansion for the time dependence of the transmission intensity is derived.

II. THEORY

A. Radiation of the Mössbauer source

We describe classically the recoilless radiation emitted by a thin Mössbauer source. Polarization of the radiation is not taken into account. The radiation is assumed to propagate in the positive x direction. The phase modulation $\varphi(t)$ may be produced by mechanical displacement. The negative frequency part $E_s(x,t)$ of the field emitted by a single line source can be described by

$$E_s(x,t) \propto \exp[-\Gamma_0(t-t_0)/2 + i\varphi(t) + i(\omega_s t - kx)] \times \Theta(t-t_0) , \tag{2.1}$$

where k is the wave number of the radiation, $\omega_s/2\pi$ is the resonance frequency of the nucleus, $1/\Gamma_0$ is the lifetime of the excited state, and t_0 is the time at which the excited state is formed. The unit step function $\Theta(t-t_0)$ is equal to 1 when $t \geq t_0$ and 0 otherwise. Since t_0 is not measured, integration over t_0 is involved in the calculation of the intensity of the radiation.

Actually only the correlation properties of the source radiation have to be known when the time dependence of the intensity transmitted through a resonance absorber is calculated. The correlation function

$$\langle E_s(x,t') E_s^*(x,t'') \rangle_{t_0} \propto \exp[-\Gamma_s | t'-t'' | /2 + i\omega_s(t'-t'') + i\varphi(t') - i\varphi(t'')] \tag{2.2}$$

can be obtained by integration over t_0. In the Appendix it is argued that, if there is line broadening in the source, Γ_0 can be replaced by an effective linewidth Γ_s. It is also possible to justify Eq. (2.2) quantum electrodynamically by describing the source radiation with a Fock state (number state).[28]

B. Response of the resonance absorber

The derivation of the absorber response resembles calculations in laser spectroscopy[29–31] with the simplification that saturation effects due to strong exciting fields can be neglected. The resonant nucleus is treated as a two-level system with the lower level $|1\rangle$ and the upper level $|2\rangle$. The Hamiltonian is of the form $\hat{H} = \hat{H}_0 + \hat{H}_1$, where $\hat{H}_0$ causes the level splitting

$$\hbar\omega_a = \langle 2 \mid \hat{H}_0 \mid 2 \rangle - \langle 1 \mid \hat{H}_0 \mid 1 \rangle \tag{2.3}$$

and the interaction term $\hat{H}_1$ induces transitions between the levels. The interaction is assumed to be proportional to the incident field. Thus the off-diagonal matrix element of the Hamiltonian is

$$\langle 1 \mid \hat{H}_1 \mid 2 \rangle = -\mu_{12} E_T(x,t) + \text{c.c.} , \tag{2.4}$$

where the real number μ_{12} is the off-diagonal element of the interaction operator $\hat{\mu}$ and $E_T(x,t)+\text{c.c.}$ is the field inside the absorber at the depth x.

The ensemble of nuclei is treated with the aid of the density operator $\hat{\rho}(x,t)$. The crystal structure of the absorber is not taken into account explicitly. The equation of motion for $\hat{\rho}$

$$i\hbar \frac{d\hat{\rho}}{dt} = [\hat{H}, \hat{\rho}] \tag{2.5}$$

is supplemented by phenomenological relaxation terms. Then the following Bloch equations are obtained:

$$\dot{\rho}_{11} - \dot{\rho}_{22} = -\Gamma_0(\rho_{11} - \rho_{22} - \Delta) - 2i\mu_{12} E_T(x,t)(\rho_{12} - \rho_{21})/\hbar , \tag{2.6a}$$

$$\dot{\rho}_{12} = (-\Gamma_a/2 + i\omega_a)\rho_{12} - i\mu_{12} E_T(x,t)(\rho_{11} - \rho_{22})/\hbar , \tag{2.6b}$$

where Δ is the population difference in the equilibrium. The relaxation term introduces the decay constants Γ_0 and $\Gamma_a = \Gamma_0 + \Gamma_\varphi$. In the absence of the external field the decay of the population difference is determined by the lifetime of the excited nuclear state. The off-diagonal elements of $\hat{\rho}$ are decaying according to Γ_a, which includes an additional decay rate Γ_φ due to various dephasing mechanisms (homogeneous and inhomogeneous). An example of these disturbances would be the dipole-dipole interaction between the absorber nuclei. It is assumed that the dephasing can be treated with a single parameter Γ_φ. The decay constants Γ_0 and Γ_a correspond to the longitudinal and transverse relaxation times T_1 and T_2^*, respectively.

In Mössbauer spectroscopy, the population difference between the lower and upper levels is given very accurately by the equilibrium value $\rho_{11} - \rho_{22} \simeq \Delta \simeq 1$, because the incident field is weak: $\mu_{12} \mid E_T \mid \ll \hbar\Gamma_0$. Then the Fourier transform of the off-diagonal element can be calculated from Eq. (2.6b):

$$\mathcal{F}\{\rho_{12}\} = \rho_{12}(x,\omega) = -\frac{\mu_{12} E_T(x,\omega)/\hbar}{\omega - \omega_a - i\Gamma_a/2} . \tag{2.7}$$

The Fourier transform of the induced polarization is

$$P(x,\omega) = \mathcal{F}\{N \,\mathrm{Tr}(\hat{\rho}\hat{\mu})\} = N\mu_{12}[\rho_{12}(x,\omega) + \rho_{12}^*(x,-\omega)] , \tag{2.8}$$

where N is the number density of the resonant nuclei. Near the resonance, $\omega \simeq \omega_a \gg \Gamma_a$, the term $\rho_{12}^*(x,-\omega)$ can be neglected (rotating-wave approximation) and it is seen that the polarization is proportional to the incident field

$$P(x,\omega) \simeq -\frac{N\mu_{12}^2/\hbar}{\omega - \omega_a - i\Gamma_a/2} E_T(x,\omega) . \tag{2.9}$$

The propagation of the field is calculated from the Maxwell equations using $P(x,\omega)$ as a source field. The wave equation

$$\frac{\partial^2 E_T(x,\omega)}{\partial x^2} = -k^2 n^2(\omega) E_T(x,\omega) \tag{2.10}$$

results, where the complex index of refraction is

$$n(\omega) \simeq 1 - \frac{N\mu_{12}^2/(2\epsilon_0\hbar)}{\omega - \omega_a - i\Gamma_a/2} . \tag{2.11}$$

Nonresonant absorption can be taken into account by adding a dissipation term to Eq. (2.10).

The absorber is situated between the planes $x=0$ and $x=L$. Taking into account the boundary condition $E_T(0,\omega) = E_s(0,\omega)$ the solution of Eq. (2.10) is given by

$$E_T(L,\omega) = e^{-ikn(\omega)L} E_s(0,\omega) = e^{ikL[1-n(\omega)]} E_s(L,\omega) , \tag{2.12}$$

where the wave traveling in the negative x direction is omitted. The absorber response is

$$a(\omega) = e^{ikL[1-n(\omega)]} = \exp[ib/(\omega - \omega_a - i\Gamma_a/2)] , \tag{2.13}$$

where $b = kLN\mu_{12}^2/(2\epsilon_0\hbar)$ is constant. The frequency spectrum transmitted through the resonance absorber of thickness L is found out by multiplying the frequency spectrum of the incoming radiation by $a(\omega)$. From now on the spatial dependencies of the fields at $x=L$ are not written out explicitly and, e.g., $E_T(\omega)$ is used for $E_T(L,\omega)$.

In Mössbauer spectroscopy relatively thick absorbers are used. Thus it is necessary to resort to the exponential response (2.13) in contrast to laser spectroscopy, where thin absorbers are often employed. The main approximations made in obtaining (2.13) are the following: low intensity of the source radiation ($\mu_{12} \mid E_T \mid \ll \hbar\Gamma_0$), sharp resonance ($\omega_a \gg \Gamma_a$), small value of $\mid 1 - n(\omega) \mid$, exclusion of the waves traveling in the negative x direction, exponential dephasing of ρ_{12}, and omission of the hyperfine interactions and the crystal structure of the absorber. The first four approximations will cause very small errors in Mössbauer spectroscopy. Although the dephasing approximation may affect the detailed form of Eq. (2.13), it will not change the basic characteristics of the absorber response (see Appendix). The above derivation assumed a single-line absorber, but the treatment could be generalized to include also the hyperfine interactions. In normal conditions omission of the crystal structure does not cause a large error in Eq. (2.13), either.

The inverse Fourier transform of the absorber response $a(\omega)$ is

$$a(t) = \delta(t) - be^{i\omega_a t - \Gamma_a t/2} \sigma(bt)\Theta(t) . \tag{2.14}$$

Here $\delta(t)$ is the Dirac delta function and $\sigma(x) = J_1(2\sqrt{x})/\sqrt{x}$. A similar response function has been derived in Ref. 32. The time dependence of the transmitted field $E_T(t)$ can be calculated as a convolution of $a(t)$

and $E_s(t)$

$$E_T(t)=\int_{-\infty}^{\infty} a(t-t')E_s(t')dt'=E_s(t)+E_a(t)\ , \tag{2.15}$$

where the total field is written as a sum of the source field and a field due to the induced polarization of the absorber (absorber field)

$$E_a(t)=-b\int_0^{\infty} e^{i\omega_a t'-\Gamma_a t'/2}\sigma(bt')E_s(t-t')dt'\ . \tag{2.16}$$

Equation (2.16) describes coherently scattered radiation, because for a thin absorber the field amplitude is proportional to the number of scatterers. As long as the inverse Fourier transform of the absorber response contains the delta function, the transmitted field can be expressed as a sum of the source field and another field due to the absorber. This decomposition is conceptually clear and it allows the identification of the various contributions on the time dependence of the transmission intensity.

Essentially the same absorber response $a(\omega)$ as that of Eq. (2.13) was found by considering an electromagnetic wave passing through a medium filled with classical resonators.[33] Also, quantum-mechanical derivations of the absorber response have been made based on the Schrödinger equation.[34,35] In Ref. 34, the discrete crystal lattice was replaced by a continuous distribution of absorber nuclei. A detailed calculation for a one-dimensional random lattice supported the validity of this procedure. Only a small correction was obtained to Eq. (2.13) due to waves traveling in the negative x direction. In Ref. 35 the refraction index of Eq. (2.11) for a cubic isotopically pure lattice was derived. Thus our semiclassical results are seen to be in agreement with these quantum-mechanical calculations.

C. Calculation of the transmission intensity

The time dependence of the recoilless radiation $N'(t)$ is obtained by integrating $|E_T(t)|^2$ over t_0:

$$N'(t)\propto\int_{-\infty}^{\infty}dt_0\int_{-\infty}^{\infty}dt'a(t-t')E_s(t')\times\int_{-\infty}^{\infty}dt''a^*(t-t'')E_s^*(t'')\ . \tag{2.17}$$

Performing the t_0 integration first results in the correlation function of Eq. (2.2), which contains all the required information about the source. Taking into account both the recoiled and recoilless portion of the radiation, the total relative intensity can be written in the form[2]

$$N(t)/N_0=\mathrm{Re}\left[1-2f_s bF_+(t)\int_{-\infty}^{t}dt'\sigma(b(t-t'))/F_+(t')+2f_s b^2 e^{-\Gamma_a t}\int_{-\infty}^{t}dt'F_-(t')\sigma(b(t-t'))\int_{-\infty}^{t'}dt''\sigma(b(t-t''))/F_+(t'')\right]\ , \tag{2.18}$$

where N_0 is the off-resonance intensity, f_s is the recoilless fraction of the source, and $F_\pm(t)=\exp[-(\Gamma_s\pm\Gamma_a)t/2-i\Delta\omega t+i\varphi(t)]$. Here $\Delta\omega=\omega_a-\omega_s$ is the shift between the source and absorber line positions. In the Appendix it is shown that without modulation [i.e., $\varphi(t)\equiv 0$] Eq. (2.18) reduces to the conventional transmission integral with

$$4b/\Gamma_0=T_a=n'\sigma_0 f_a\ , \tag{2.19}$$

where T_a is the Mössbauer thickness of the absorber, n' is the number of resonant nuclei per unit area, σ_0 is the cross section of resonance absorption, and f_a is the recoilless fraction of the absorber.

The three terms inside the large parentheses in Eq. (2.18) can be identified in terms of the fields $E_s(t)$ and $E_a(t)$ of Eq. (2.15). The constant term on the right-hand side consists of the square of the source field, $|E_s(t)|^2$, and of the nonresonant background intensity. The second term describes the interference $E_s(t)E_a^*(t)$ between the source and absorber fields. With a thin absorber the interference term is proportional to b, because the argument $b(t-t')$ in the integrand mainly influences the time dependence of this term. The third term is proportional to b^2 and it corresponds to the square of the absorber field $|E_a(t)|^2$. All these terms turn out to be necessary in the analysis of TM measurements with practical absorber thicknesses. Note that the second term reacts instantaneously to rapid changes in $\varphi(t)$, whereas the third term has a delay because of the t' integration. In the following the time dependence of the transmission intensity will be calculated corresponding to several shapes and frequencies of the phase modulation $\varphi(t)$. Equation (2.18) will be particularly useful as a starting point for these calculations.

We conclude this section with a brief comment on transient effects in scattering geometry. The polarization of Eq. (2.9) may be interpreted as a scattering amplitude, which can be used, e.g., in calculating the conversion electron transients. Thus the third term of Eq. (2.18) gives the first approximation for the time dependence of the scattering transients. Examples will be given by the terms proportional to b^2 in Eqs. (3.7), (3.16), and (3.20) which describe the intensity for thin scatterers.

III. APPLICATIONS OF THE THEORY

A. Different experimental regions

1. *Conventional measurements*

In conventional Mössbauer measurements periodical Doppler modulation $\dot{\varphi}(t)=k\dot{x}(t)$ is used, where $\dot{x}(t)$ is the Doppler velocity between the source and absorber and the dots denote time derivatives. The frequency (and amplitude) of the modulation are small and thus the change in the Doppler velocity during the lifetime of the excited nuclear state is much less than the linewidth in velocity units. The lifetimes of the ^{57}Fe and ^{67}Zn Mössbauer states are about 140 ns and 13 μs, respectively. These two isotopes are the ones mainly considered in the following.

The transmission intensity as a function of the Doppler velocity is given by the conventional transmission integral. A deviation from this line shape appears when the modulation frequency or amplitude is increased, so that the resonance is passed in a time comparable to the lifetime of the excited state.[1] Then the transmission intensity at time t depends on the history of the Doppler velocity and the modulation is simplest to treat as phase modulation $\varphi(t)$.

We calculate the line shape for a thin absorber $b/\Gamma_a < 1$. Then the approximation

$$\sigma(bt) \simeq \exp(-bt/2) \tag{3.1}$$

can be used in Eq. (2.14) with good accuracy, since the discrepancy in the most critical region $0 \leq bt < 1$ is smaller than 0.03. This approximation increases the linewidth of the absorber from Γ_a to $\Gamma_a + b$ (thickness broadening). Using Eq. (3.1) the shape of the transmission curve is obtained from the first and second terms of Eq. (2.18), as the Taylor-series expansion of $\varphi(t')$ around the point $t' = t$ is truncated after the quadratic term,

$$\frac{N(t)}{N_0} \simeq 1 - \frac{2f_s b}{\Gamma_T} \int_0^\infty dx\, e^{-x} \cos\left[\frac{\ddot{\varphi}(t_r)}{2\Gamma_T^2} x^2 + \frac{\Delta\omega - \dot{\varphi}(t)}{\Gamma_T} x \right]. \tag{3.2}$$

Here $2\Gamma_T = \Gamma_s + \Gamma_a + b$ is the total linewidth and t_r is the time at which the system is in resonance: $\dot{\varphi}(t_r) = \Delta\omega$. There are usually two values t_r during the period of the modulation satisfying this condition. It is assumed that the acceleration is approximately constant within the resonance line implying that $\ddot{\varphi}(t) \simeq \ddot{\varphi}(t_r)$. The main effect of the third term in Eq. (2.18) is to saturate the absorption. The deviation from the Lorentzian line shape is determined by a distortion parameter

$$d = |\ddot{\varphi}(t_r)| / \Gamma_T^2 , \tag{3.3}$$

which is inversely proportional to the square of the experimental linewidth. A thickness-broadened Lorentzian as a function of $\dot{\varphi}(t)$ results when $\ddot{\varphi}(t_r)$ is omitted in Eq. (3.2). The linewidth $2\Gamma_T$ is close to conventionally used approximations.[36]

By examining Eq. (3.2) it turns out that the time of minimum transmission $t_{\min}$ is delayed from t_r. The magnitude of the delay is constant in time: $t_{\min} - t_r \simeq \frac{3}{2}\Gamma_T^{-1}$. The observation of this delay becomes easier as d is increased. Another time-dependent deviation from the Lorentzian line shape is the asymmetry of the transmission curve: the absorption changes more slowly before $t_{\min}$ than after it. Thus the apparent width of the first half of the distorted line (Γ_1) is larger than that of the second half (Γ_2). In Fig. 1, Γ_1, Γ_2, and their average are shown as a function of d. With $d \lesssim 0.1$, the asymmetry is given by

$$(\Gamma_1 - \Gamma_2)/(\Gamma_1 + \Gamma_2) \simeq d , \tag{3.4}$$

whereas the increase in the average linewidth is proportional to d^2.

As an example of measurements, where these distortions may occur, we take an ^{57}Fe spectrum with natural linewidths and with a maximum velocity of 10 mm/s. When the Doppler modulation is sinusoidal at a frequency of 100 Hz, the distortion parameter is $d \simeq 0.01$ and an asymmetry of 1% (0.002 mm/s) is expected for lines near zero velocity (see also Sec. III A 4). Conventionally the data of a Mössbauer experiment are folded, i.e., the contents of the data channels corresponding to equal Doppler velocities are summed up. Folding decreases the distortions and, in principle, the line positions on the energy scale are not affected. In any case, for a reliable analysis of conventional Mössbauer experiments the distortion parameter should be considerably smaller than 1.

2. *Transient experiments*

As d is increased close to 1, the asymmetry gradually increases and finally interference oscillations appear. Due to the oscillations the peak-to-peak effect is larger in transient experiments than in conventional measurements. We calculate the approximate time dependence of the transmission intensity when the resonance is passed rapidly: $d > 1$. If accurate quantitative results are required with $d \simeq 1$, one should use the general equation (2.18).

The integral in the second term of Eq. (2.18) can be approximated by using the Taylor-series expansion of $\varphi(t')$ around the point $t' = t_r$. Truncating the series after the quadratic term and noting that $\dot{\varphi}(t_r) = \Delta\omega$ the integral

$$\begin{aligned} &\int_{-\infty}^{t} \sigma(b(t-t')) \exp[\Gamma_{sa} t' - i\ddot{\varphi}(t_r)(t'-t_r)^2/2]\, dt' \\ &\quad \simeq \exp(\Gamma_{sa} t_r)\, \sigma(b(t-t_r)) \\ &\qquad \times \int_{-\infty}^{t} \exp[-i\ddot{\varphi}(t_r)(t'-t_r)^2/2]\, dt' \end{aligned} \tag{3.5}$$

results, where $\Gamma_{sa} = (\Gamma_s + \Gamma_a)/2$. The latter form is valid for $t - t_r > \ddot{\varphi}(t_r)^{-1/2}$, because $\sigma(b(t-t'))\exp(\Gamma_{sa} t')$ is a slowly varying function of t' as compared to $\exp[-i\ddot{\varphi}(t_r)(t'-t_r)^2/2]$. The major contribution to the integral originates in the vicinity of the point $t' = t_r$, since elsewhere the rapid oscillations average to zero. The remaining integration can be performed with the aid of Fresnel integrals C and S (Ref. 37),

$$\begin{aligned} &\int_{-\infty}^{t} \exp[-i\ddot{\varphi}(t_r)(t'-t_r)^2/2]\, dt' \\ &\quad = [\pi/\ddot{\varphi}(t_r)]^{1/2} [e^{-i\pi/4}/\sqrt{2} + C(\tau) - iS(\tau)] , \end{aligned} \tag{3.6}$$

where $\tau = [\ddot{\varphi}(t_r)/\pi]^{1/2}(t - t_r)$. It is assumed that $\ddot{\varphi}(t_r)$ is positive, but this is not an essential limitation.

The integrals of the third term of Eq. (2.18) can be evaluated similarly with the final result

$$\begin{aligned} N(t)/N_0 \simeq 1 &- f_s b \left[\frac{8\pi}{\ddot{\varphi}(t_r)} \right]^{1/2} \sigma(b(t-t_r)) e^{-\Gamma_{sa}(t-t_r)} \left[\cos[\varphi(t) - \varphi(t_r) - \Delta\omega(t-t_r) - \tfrac{1}{4}\pi] - \frac{g(\tau)}{\sqrt{2}} \right] \\ &+ \frac{2\pi f_s b^2}{\ddot{\varphi}(t_r)} \sigma^2(b(t-t_r)) e^{-\Gamma_a(t-t_r)} \left[C(\tau) + S(\tau) + \int_\tau^\infty g(x)\, dx \right] , \end{aligned} \tag{3.7}$$

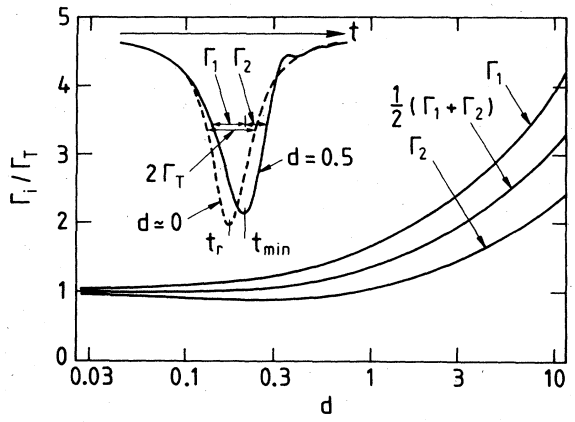

FIG. 1. Apparent half-widths Γ_1 and Γ_2 of the resonance line, calculated from Eq. (3.2) as a function of d. Distortion parameter d is proportional to the rate of change of the Doppler velocity at the resonance. Full width at half maximum of the undistorted line is $2\Gamma_T$. With $d \gtrsim 1$, interference oscillations appear after the resonance line.

where

$$g(\tau)=[\tfrac{1}{2}-C(\tau)]\cos(\pi\tau^2/2)+[\tfrac{1}{2}-S(\tau)]\sin(\pi\tau^2/2)$$

(Ref. 37). Equation (3.7) is useful in estimating the result of a TM experiment at modulation frequencies smaller than the linewidth. It is applicable also to thick absorbers. There are generally two transients of the form of Eq. (3.7) during one period of the modulation.

The second term of Eq. (3.7) describes the interference oscillations between the source field and the field due to the polarization of the absorber (FID). The magnitude of the correction $-g(\tau)/\sqrt{2}$ is about 0.1 at $\tau=1/\sqrt{\pi}$ and it decreases rapidly with larger τ. The third term corresponds to the square of the absorber field. The sum of the Fresnel integrals shows damped oscillations around the average value 1 with a maximum amplitude of ~ 0.3 at $\tau=1/\sqrt{\pi}$. The integral of the function g produces a small correction. The oscillations of the second and third terms of Eq. (3.7) have a relative phase shift of 90°. Using the approximation (3.1) it is seen that the second term is decaying by the time constant Γ_T and the third term by Γ_a+b.

In the following we compare the information obtainable from conventional and transient Mössbauer measurements. The phase modulation $\varphi(t)$ is assumed to have a period $1/f=2\pi/\Omega$ and an amplitude (modulation index) a. The sinusoidal wave form

$$\varphi(t)=a\sin(\Omega t) \tag{3.8}$$

is used in the experiments to be described later in this paper. When the modulation is produced by moving the source, the displacement amplitude is $x_0=a\lambda$, where $\lambda=2\pi\lambda$ is the wavelength of the radiation. The displacement amplitude can be determined from the time dependence of the interference oscillations described by the second term of Eq. (3.7). This calibration is absolute in terms of the wavelength λ. The center shift $\Delta\omega$ is determined by the relative position of the two transients observed during the period of the modulation.

Conventional transmission curves with the total linewidth of $3.6\Gamma_0$ are shown in Fig. 2(a). The curves have been calculated according to Eq. (A10) of the Appendix. In two cases there is an excess line broadening of $0.5\Gamma_0$ in the source or in the absorber and in the third case the line is broadened by the increased absorber thickness. The curves have been scaled in such a way that the extrema of the spectra coincide. The shapes of the curves are very similar, which makes it difficult to determine the thickness of the absorber b and the linewidths Γ_s and Γ_a from this kind of a conventional Mössbauer spectrum. If Γ_s, Γ_a, and b were known, f_s could be determined from the absorption after the background correction.

The corresponding TM curves calculated according to Eq. (2.18) are presented in Fig. 2(b). They show distinguished differences in the time dependence of the transmission intensity. The recoilless fraction of the source can now be obtained from the peak-to-peak effect, because the parameters Γ_s, Γ_a, and b are determined by the shape of the transmission curve. From the thickness parameter b the recoilless fraction of the absorber can be calculated using Eq. (2.19). Thus all the parameters f_s, f_a, Γ_s, and Γ_a can be extracted from a single TM measurement. It should also be noted that the fitted values of the linewidths and line positions are obtained in terms of the modulation frequency, which is usually known very

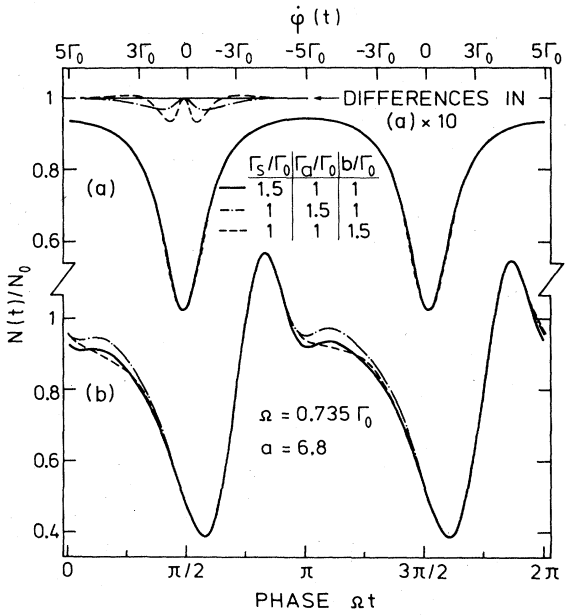

FIG. 2. Conventional transmission curves (a) and transient curves with $d=1.2$ (b) plotted unfolded as a function of the phase Ωt of the sinusoidal modulation. Maximum velocity corresponds to five natural linewidths and the center shift is $\Delta\omega=0.2\Gamma_0$ in all curves. Vertical scale applies to the case $\Gamma_s/\Gamma_0=1.5$. Linewidth of the source (absorber) is Γ_s (Γ_a) and the parameter b describes the thickness of the absorber. Transient curves are more sensitive to changes in the parameters affecting the linewidth than the conventional Mössbauer spectra. Transmission intensity is given in terms of the recoilless fraction of the source in Figs. 2, 4, and 5.

accurately. In conventional measurements the linewidths and line positions are determined in terms of the maximum velocity, which is more difficult to calibrate.

3. High-frequency experiments

High-frequency experiments have been considered earlier by Monahan and Perlow.[7] We extend their results to phase modulation of arbitrary shape and derive a simple expression for the time dependence of the transmission intensity applicable also to thick absorbers.[10] The modulation frequency is assumed to be large, i.e., $\Omega \gg \Gamma_T$ and the line position is written in the form $\Delta\omega = j\Omega + \xi$, which allows one to study the contribution of spectral lines at large velocities. Here j is an integer and ξ is a deviation of the line position from the nearest sideband j. After the Fourier-series expansion of Eq. (A1) is substituted into Eq. (2.18) the interference term

$$2f_s b F_+(t) \sum_{n=-\infty}^{\infty} C_n^* \int_{-\infty}^{t} dt' \exp[\Gamma_{sa} t' + i(j-n)\Omega t' + i\xi t'] \sigma(b(t-t'))$$

$$= 2f_s e^{i\varphi(t)} \sum_{n=-\infty}^{\infty} C_n^* e^{-in\Omega t} (1 - \exp\{-b/[\Gamma_{sa} + i(j-n)\Omega + i\xi]\}) \quad (3.9)$$

can be integrated.[38] Here only the largest term $n = j$ need to be retained.

Similar considerations apply to the third term of Eq. (2.18), which is found to be independent of time. The final result is

$$N(t)/N_0 \simeq 1 - A(\xi) |C_j|^2 + 2f_s \mathrm{Re}[C_j^* \{1 - \exp[-b/(\Gamma_{sa} + i\xi)]\} \times (C_j - \exp\{i[\varphi(t) - j\Omega t]\})] , \quad (3.10)$$

where $A(\xi)$ is the absorption that would be measured at the distance ξ from the center of the line. The time dependence of the transmission intensity consists of the phase modulation $\varphi(t)$ and of the oscillation at the sideband frequency $j\Omega/2\pi$. Equation (3.10) is an extension of the result presented in Ref. 10, where it was assumed that $j = 0$. When $\Delta\omega \simeq 0$ and C_0 is real, the time dependence is of the form

$$N(t) \propto \cos\varphi(t) . \quad (3.11)$$

With the sinusoidal modulation of Eq. (3.8), the oscillations in the transmission intensity are called quantum beats.[6]

If the source or absorber has several lines, the interference oscillations due to these lines may be mixed in the high-frequency experiments. Assume for simplicity that the conventional Mössbauer spectrum consists of two clearly separated lines of equal absorption. The first line is at zero velocity and the second line is at the position $\Delta\omega = j\Omega + \xi$. The contribution of these lines on the time dependence of the transmission intensity can be estimated using Eq. (3.10). If $\xi \gg \Gamma_T$, the time dependence due to the second line is negligible. When sinusoidal modulation is used, the contribution of the second line is proportional to $C_j = J_j(a)$ and it can have an appreciable value only if $a \gtrsim j$, i.e., $a\Omega \gtrsim \Delta\omega$. The interpretation of this condition is that the maximum velocity must be at least as large as the separation of the lines. If we specially choose an amplitude which is a zero of J_j (J_0), only the contribution of the first (second) line is seen.

4. Practical considerations

The various experimental conditions considered above are summarized on the frequency-velocity plane of Fig. 3. On the vertical scale $\dot{\varphi}_{\max}$ is the rate of the phase change corresponding to the maximum Doppler velocity. Separate frequency and velocity scales are provided for the resonances of ^{57}Fe and ^{67}Zn. Sinusoidal modulation and a resonance line of natural width at zero velocity are assumed. Then the distortion parameter is given by $d = d_0 = a\Omega^2/\Gamma_0^2$. The borders of the transient region are determined by the conditions $d_0 \gtrsim 0.3$ and $\Omega/\Gamma_0 \lesssim 3$. The latter condition states that the modulation frequency must be small enough to allow considerable decay of the transients. The high-frequency region is bounded by $\Omega/\Gamma_0 \gtrsim 3$.

Most ^{57}Fe measurements have been performed at relatively low modulation frequencies ($f < 100$ Hz) with maximum velocities less than 20 mm/s. With ^{57}Fe, transient effects would be very difficult to observe at frequencies below 1 kHz. Measurements with ^{67}Zn are experimentally

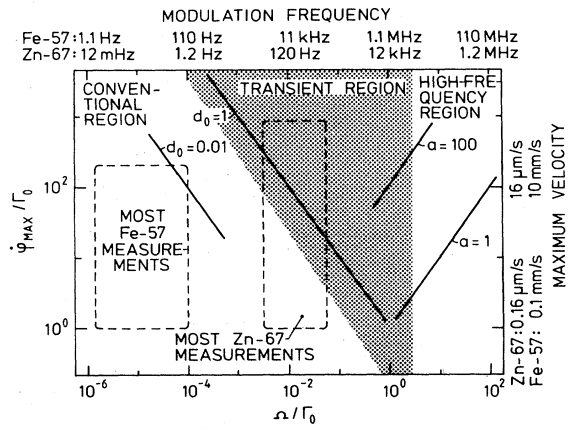

FIG. 3. Frequency-velocity plane for classification of Mössbauer measurements. Sinusoidal modulation and a resonance line of natural width at zero velocity are assumed. Amplitude of the phase modulation is a (modulation index) and the distortion parameter $d_0 = a\Omega^2/\Gamma_0^2$ describes the acceleration of the drive motion in terms of the natural linewidth.

easiest to perform at frequencies of about 100 Hz. The largest maximum velocities have been ~ 200 μm/s. In several conventional ^{67}Zn experiments reported, the distortion parameter corresponding to the natural linewidth (d_0) has been considerably larger than 1. However, the transient effects have been diminished by large experimental linewidths and isomer shifts. The asymmetry of the resonance lines is also decreased by folding of the data. The distortions due to time-dependent effects will become significant if the excess line broadenings present in many ^{67}Zn measurements can be eliminated.

B. Phase switching

1. Ideal modulation

Ideal phase switching is of the form $\varphi(t)=\Delta\varphi\Theta(t)$, where $\Delta\varphi=\Delta x/\lambda\!\!\!^{-}$ is the phase change due to a sudden displacement Δx at time $t=0$. For the ^{67}Zn resonance $\lambda\!\!\!^{-}\simeq 2.1$ pm and thus very small displacements are adequate for phase switching. By substituting $x=b(t-t')$ and $y=b(t-t'')$ in Eq. (2.18) the transmission intensity can be written in an integral form

$$N(t)=N(t<0)+2f_sN_0\mathrm{Re}\left[(1-e^{i\Delta\varphi})\left[1-\int_0^{bt}dy\,\sigma(y)e^{\beta^- y}\right]\int_{bt}^{\infty}dx\,\sigma(x)e^{-\beta^+ x}\right]\Theta(t)\,, \tag{3.12}$$

where

$$\beta^{\pm}=[(\Gamma_s\pm\Gamma_a)/2+i\,\Delta\omega]/b \tag{3.13}$$

and $N(t<0)$ is the steady-state value of the transmission intensity.

The integrals of Eq. (3.12) can be evaluated in terms of a series expansion of Bessel functions with the final result

$$N(t)=N(t<0)+2f_sN_0\mathrm{Re}\{(1-e^{i\Delta\varphi})S(bt;-\beta^-)[e^{-\Gamma_a t}S(bt;\beta^+)-e^{-1/\beta^+ +\beta^- bt}]\}\Theta(t)\,, \tag{3.14}$$

where

$$S(x;\beta)=\sum_{k=0}^{\infty}J_k(2\sqrt{x})(\beta\sqrt{x})^k \tag{3.15a}$$

$$=e^{-1/\beta+\beta x}-\sum_{k=1}^{\infty}(-1)^kJ_k(2\sqrt{x})(1/\beta\sqrt{x})^k\,. \tag{3.15b}$$

The series expansion of Eq. (3.15a) converges rapidly with $|\beta\sqrt{x}|<1$. Equation (3.15b) is obtained from the formula for generating Bessel functions and it is to be used with $|\beta\sqrt{x}|>1$. Ideally there is no time dependence in the transmission intensity, when the phase shift is $\Delta\varphi=2n\pi$, i.e., when the displacement Δx is an integer multiple of the wavelength.

At time $t=0$ the transmission intensity changes sharply if $\Delta\varphi\neq 2n\pi$. After the initial change the intensity returns back to the steady-state value according to Eq. (3.14). For a thin absorber the time dependence of the transmission intensity is given by

$$N(t)\simeq N(t<0)+2N_0f_sb\,\mathrm{Re}\left[(1-e^{i\Delta\varphi})\frac{e^{-\Gamma_T t-i\Delta\omega t}}{\Gamma_T+i\,\Delta\omega}\left[1-b\frac{1-e^{-\Gamma_d t+i\Delta\omega t}}{\Gamma_d-i\,\Delta\omega}\right]\right]\Theta(t)\,, \tag{3.16}$$

where $\Gamma_d=(\Gamma_a+b-\Gamma_s)/2$. The decay is approximately exponential if $\Delta\omega\simeq 0$.

Some calculated transmission curves with a very thick absorber are shown in Fig. 4. For a thick absorber and small center shift the decay

$$N(t)\simeq N(t<0)+2f_sN_0[1-\cos(\Delta\varphi)]J_0^2(2\sqrt{bt})$$

$$\times\exp(-\Gamma_a t)\Theta(t) \tag{3.17}$$

is oscillatory due to the square of the Bessel function J_0^2 (curve a in Fig. 4). The effect is largest when the value of $\Delta\omega$ is near the linewidth (curve b). As the center shift is still increased, oscillations at the angular frequency $\Delta\omega$ also become visible (curve c).

Because $S(0;\beta)=1$, the magnitude of the relative intensity change at $t=0$ is

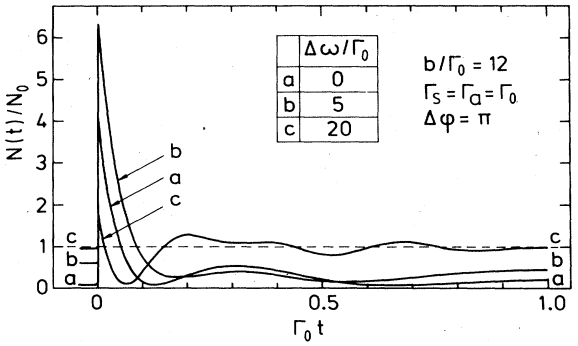

FIG. 4. Time dependence of the transmission intensity due to a sudden phase shift $\Delta\phi=\pi$ at time $t=0$, calculated according to Eq. (3.14). The horizontal scale is given in terms of the lifetime of the excited state ($1/\Gamma_0$). Curves with three different values of the center shift $\Delta\omega$ are shown. In conventional Mössbauer measurements the transmission intensity would vary between zero and the dashed line.

$$\frac{\Delta N}{N_0} \equiv \frac{N(0)-N(t<0)}{N_0} = 2f_s \mathrm{Re}[(1-e^{i\Delta\varphi})(1-e^{-1/\beta^+})] \ . \tag{3.18}$$

If $\Delta\varphi \neq n\pi$ and $\Delta\omega \neq 0$, the value of $\Delta N/N_0$ depends on the direction of the motion of the source. The maximum value of $\Delta N/N_0$ is achieved with $\Delta\varphi=(2n+1)\pi$ when the center shift is small: the maximum relative intensity change is $4f_s$ for a thick absorber. This is 4 times the largest possible peak-to-peak effect in conventional measurements. In Fig. 5, the dependence of $\Delta N/N_0$ on the ratio $\Delta\omega/\Gamma_{sa}$ is shown with different values of b/Γ_{sa}. The largest values of $\Delta N/N_0$ are obtained with $\Delta\omega \simeq b/\pi \gg \Gamma_{sa}$. In principle, an intensity change of $\Delta N/N_0 = 8f_s$ can be obtained in phase-switching experiments.

2. *Nonidealities in the phase switching*

In the previous calculations it was assumed that the phase switching is instantaneous. In practice the rise time Δt is finite and the phase is changing with some average velocity $\langle \dot{\varphi}(t) \rangle \sim \Delta\varphi/\Delta t$. In the following we shall first discuss transients caused by changes in the angular velocity $\dot{\varphi}(t)$ (frequency switching). The results can be applied to predict the effects of the finite rise time on the phase switching.

Let us assume that the source and the absorber are first in resonance ($\Delta\omega=0$), and then at time $t=0$ the angular frequency of the source radiation is switched by an amount $\Delta\Omega > \Gamma_T$. Thus the phase modulation is of the form

$$\varphi(t) = \Delta\Omega\, t\Theta(t) \ . \tag{3.19}$$

We use the approximation of Eq. (3.1) in Eq. (2.18) in calculating the transmission intensity

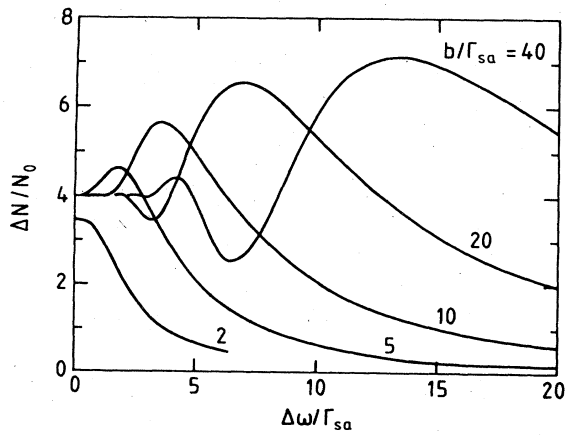

FIG. 5. Magnitude of the intensity change $\Delta N/N_0$ caused by a sudden phase shift $\Delta\varphi=\pi$, calculated according to Eq. (3.18) as a function of the center shift $\Delta\omega$. Parameters are scaled by $\Gamma_{sa}=(\Gamma_s+\Gamma_a)/2$.

$$\frac{N(t)}{N_0} \simeq 1 - \frac{2f_s b}{\Gamma_T} e^{-\Gamma_T t}\cos(\Delta\Omega\, t - \Gamma_T/\Delta\Omega) + \frac{2f_s b^2}{\Gamma_T}\left[\frac{e^{-(\Gamma_a+b)t}}{\Gamma_a+b} + \frac{e^{-\Gamma_T t}}{\Delta\Omega}\sin(\Delta\Omega\, t)\right] , \tag{3.20}$$

which is valid for $t>0$. Terms smaller than $O(\Gamma_T/\Delta\Omega)$ have been neglected. The time dependence of this transient resembles the transient excited by a rapid sweep through the resonance [Eq. (3.7)]. The oscillations appear at the frequency corresponding to the difference in the frequencies of the source and absorber fields.

The transmission intensity of Eq. (3.20) reaches a maximum value at about $\Delta\Omega\, t \simeq \pi$. The source moves half a wavelength during this interval. Correspondingly, the intensity reaches a minimum when $\Delta\Omega\, t \simeq 2\pi$. Thus the time dependence does not vanish in phase-switching experiments with $\Delta\varphi=2n\pi$ and $\Delta t>0$, but there are n interference oscillations in the transmission intensity. As large intensity changes as in the case of the ideal phase switching can be achieved, if the damping during the phase shift is negligible. In the case of Fig. 4 this means that the rise time should be smaller than $0.01\ \Gamma_0^{-1}$. The time resolution of the measuring system ought to be better than the rise time.

When periodical phase switching is used, some harmonic of the modulation frequency may coincide with a mechanical resonance frequency of the drive $\Omega_q/2\pi$. Then, in addition to the stepwise motion, the source vibrates sinusoidally at the resonance frequency with an amplitude $a_q\lambda$ which may be slightly time dependent. The frequency of the phase switching is assumed to be small, $\Omega < \Gamma_T$, and the resonance frequency is assumed to be large, $\Omega_q \gg \Gamma_T$. The phase modulation is of the form

$$\varphi(t) = \Delta\varphi\,\Theta(t) + a_q \sin(\Omega_q t) \ , \tag{3.21}$$

where the periodicity of the phase switching and damping of the mechanical oscillations are not taken into account. To simplify, we assume that $\Delta\omega=0$, use approximation (3.1) and integrate the second term of Eq. (2.18) with the result ($t>0$)

$$\frac{N(t)}{N_0} \simeq 1 - \frac{2f_s b}{\Gamma_T}\{e^{-\Gamma_T t} J_0(a_q)\cos[a_q \sin(\Omega_q t) + \Delta\varphi] + J_0(a_q)(1-e^{-\Gamma_T t})\cos[a_q \sin(\Omega_q t)]\} \ . \tag{3.22}$$

When $t \gg \Gamma_T^{-1}$, only the quantum-beat oscillations $\cos[a_q \sin(\Omega_q t)]$ remain in accordance with Eq. (3.11).

The phase-switching experiments with $\Delta\varphi \simeq \pi/2 + n\pi$ are more sensitive to small disturbances than those with $\Delta\varphi \simeq n\pi$. With these phase shifts the oscillation amplitudes of the transmission intensity are proportional to a_q and a_q^2, respectively. The nonoscillating term $-2f_s b J_0^2(a_q)/\Gamma_T$ arising from the last term of Eq. (3.22) causes a slow drift in the transmission intensity, if a_q decays slowly after the excitation.

Throughout this section it has been assumed that the

amplitude and phase of the motion have well-defined values over the volume of the source. This assumption is usually justified when the drive is operated much below its lowest mechanical resonance. Large distributions in the modulation amplitude or phase would destroy the oscillations of Eqs. (3.7), (3.10), (3.20), and (3.22) and decrease the peak-to-peak effect considerably. However, in the case of phase switching even a completely random distribution of $\Delta\varphi$ would not decrease the effect more than by a factor of 2 when the center shift is small.

IV. EXPERIMENTAL

So far only ^{57}Fe and ^{67}Zn resonances have been used in transient Mössbauer experiments. Most of the experimental data presented here were obtained using the Mössbauer resonance of ^{67}Zn. The sources were ^{67}Ga:*ZnO* single crystals containing ^{67}Zn in natural abundance. They were cylindrical in shape with a diameter of $\sim$4 mm and a thickness of $\sim$0.5 mm. The *c* axes of the hexagonal ZnO crystals[39] were perpendicular to the large surfaces. The ^{67}Ga activity was produced by 10-MeV deuteron bombardment with a typical dose of about 30 μAh. After the irradiation the crystals were annealed in an oxygen atmosphere at 700°C for about 10 h and thereafter slowly cooled to room temperature. The absorbers were made of ^{67}ZnO powder material enriched up to 87.9(7)% in ^{67}Zn. The enriched material was used as received from the supplier.[40] The grain size of the powder was between 1 and 2 μm.[41] The absorbers typically contained 1 g/cm^2 of ^{67}Zn.

With the *c* axis parallel to the direction of observation of the γ radiation, the Mössbauer spectrum of the ZnO single crystal versus ZnO powder consists of five absorption lines (Fig. 6). The separation of the lines due to quadrupole splitting is about 4.8 μm/s$\hat{=}$360 kHz (Refs. 42 and 43). This separation is considerably larger than the minimum observable linewidth $2\Gamma_0\hat{=}0.32$ μm/s. Only the center line close to zero velocity was scanned in most measurements presented in this work.

A relation between the Mössbauer thickness of the center line (T_a) and the mass of enriched ZnO per unit area (D) is obtained from Eq. (2.19) for our powder material:

$$T_a = 106(3) f_a D/(1\ \text{g/cm}^2)\ . \tag{4.1}$$

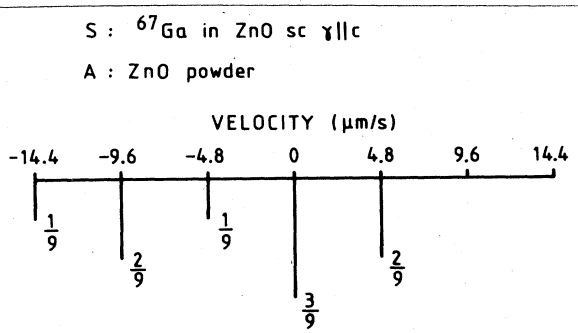

FIG. 6. Schematic ^{67}Zn Mössbauer spectrum of a ZnO single-crystal source and a thin ZnO-powder absorber. Direction of observation of the γ radiation is parallel to the *c* axis of the single crystal.

The thickness of the center line is one third of the total thickness. The uncertainty in the numerical factor is mainly due to the uncertainty in the cross section σ_0.[44] Two different thicknesses are generally needed to describe a certain resonance line of a single-crystal absorber.[45] On the other hand, a powder absorber can be treated with a single thickness parameter, independent of the polarization of the incident radiation. This is an important property for the transient experiments, in which T_a has a much greater influence on the shape of the transmission curves than in conventional Mössbauer measurements.

The experimental setup is presented in Fig. 7. The double-drive system, including both the high-frequency (hf) and the low-frequency (lf) drives, was located in a liquid-helium cryostat. The source was fixed with silicon grease on the high-frequency drive and both were clamped between styrofoam supports to prevent mechanical contact with the surrounding brass holder. The high-frequency drive unit was pressed with a Be-Cu spring against the low-frequency drive. The leads to the two drives (transducers) were flexible coaxial cables. The absorber was rigidly attached to the support of the double-drive system. The drives and the absorber were enclosed in a chamber containing gaseous helium.

The γ radiation was detected with a 3-mm-thick NaI(Tl) scintillator, the output signal of which was processed by conventional pulse electronics. The shaping time of the linear amplifier was 0.25 μs. The counting rate in the 93-keV energy window was typically 40 000 s^{-1} at the beginning of the measurement.

In TM measurements the counts were collected with a time-to-digital converter (TDC).[46] The TDC permits use

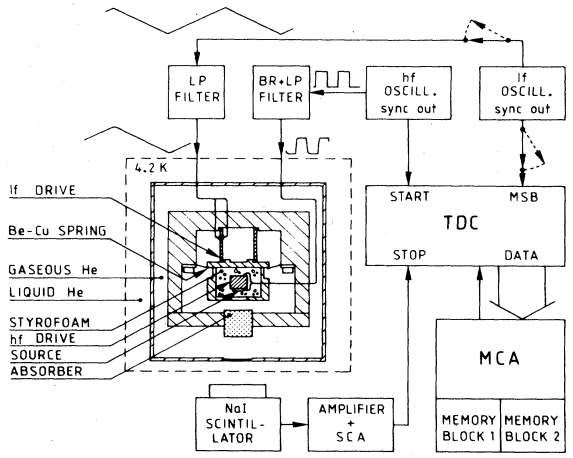

FIG. 7. Experimental setup for transient Mössbauer measurements with ^{67}Zn. The system includes separate drives for the high-frequency (hf) modulation and for the optional low-frequency (lf) modulation. Time-to-digital converter (TDC) transfers the digitized time interval between the start and stop pulses to the multichannel analyzer (MCA). The most-significant-bit (MSB) input determines the memory block to be used. Waveforms presented are those of phase-switching experiments. Low-pass (LP) and band-reject (BR) filters are used to avoid excitation of the mechanical resonances of the drives. Measurements were performed at liquid-helium temperature.

of channel advance times as short as 150 ns with a differential nonlinearity much less than 0.1%. The synchronizing output of the oscillator driving the high frequency transducer is used to produce start pulses which clear a synchronous counter. The signal caused by a detected γ quantum is used as a stop pulse to read the output of the counter. The TDC also contains a data buffer, which enables practically zero-dead-time operation even at the highest counting rates used. The buffer is accomplished with the aid of a 16×10-bit FIFO (first-in—first-out) memory. The optional MSB input determines the most-significant bit of the data transferred to the multichannel analyzer (MCA). This makes possible the measurement of two transient curves corresponding to the two opposite slopes (velocities) of the triangular low-frequency motion. In most TM measurements only the high-frequency drive was employed. In conventional Mössbauer measurements the low-frequency drive was used. The data were collected directly to the MCA operated in the multiscaling mode.

We next consider the transducers in more detail. The high-frequency transducer was either a lead zirconate titanate (PZT-5A) plate[47] or a quartz plate.[48] The thickness and diameter of the PZT transducer were 2 and 6 mm and the corresponding dimensions of the quartz transducer were 5 and 6 mm. The voltage-to-displacement conversion factor of PZT (60 pm/V) is about 50 times larger than that of quartz (1.3 pm/V) at liquid-helium temperature. Since the ZnO crystal itself is piezoelectric, it was covered with silver paint when the quartz transducer was used.

The piezoelectricity of the ZnO source crystal was utilized in studying the mechanical resonances of the quartz drive in the actual measurement conditions. The lower surface of the high-frequency drive to which the source was attached served as a common electrode. The voltage amplitude over the ZnO crystal measured as a function of the vibration frequency of the quartz transducer revealed the mechanical resonances. The lowest resonance was at 433 kHz and its full width at half maximum was 10 kHz.

The resonance frequencies of the PZT transducers are easy to find by monitoring the driving voltage as a function of the vibration frequency. At the resonance the absorption of electrical power is increased significantly. The lowest mechanical resonance of the high-frequency PZT transducer was at 340 kHz. The method of monitoring the driving voltage is not useful in the case of the quartz transducer, since the capacitance of the quartz plate is much smaller than that of the coaxial cable inside the cryostat. The mechanical resonance frequencies of the drives can also be found through Mössbauer measurements. At the resonance the time average of the transmission intensity increases sharply, as the vibration frequency is varied.

The phase-switching measurements were performed with square-wave-shaped driving voltage at a frequency of 19.5 kHz. Passive low-pass and band-reject filters were used to prevent excitation of the mechanical resonances of the drive (Fig. 7). Filtering increased the time constant of the phase switching to about 1 μs. The use of the quartz transducer was advantageous in phase-switching experiments, since the lowest mechanical resonance of the quartz drive was at a higher frequency than that of the PZT drive. The operating frequencies of the high-frequency drives range from a few kilohertz to above 100 kHz when sinusoidal modulation is used. Even with sinusoidal voltage the mechanical resonances may be excited due to harmonics inevitably produced by any function generator.

The low-frequency transducer was a PZT-4 tube.[47] The height and outer diameter of the tube were 12.7 mm and the wall thickness was 0.8 mm. The low-frequency drive is similar to that first used by Griesinger *et al.*[49] The lowest resonance frequency was at ~5 kHz, and the voltage-to-displacement conversion factor was 0.53 nm/V. In conventional measurements the low-frequency drive was operated with sinusoidal voltage at a frequency of 130 Hz. The additional center shifts required were produced using low-pass-filtered triangular voltage at a frequency of 20 Hz.

The properties of a PZT-4 low-frequency transducer have been studied with a superconducting quantum interference device (SQUID) based displacement sensor.[50] The resolution of the sensor was 8×10^{-15} m/$\sqrt{\text{Hz}}$ in the frequency band from almost dc to 10 kHz. The transducer was found to be suitable for ^{67}Zn Mössbauer experiments with sinusoidal modulation at frequencies up to a few kilohertz. Triangular motion of good quality could be produced at the frequencies and amplitudes studied ($f\lesssim100$ Hz, $x_0\lesssim1$ nm).

Transient experiments were also performed with ^{57}Fe. In these measurements the source was a small piece of a ^{57}Co:*Rh* foil. The foil was glued on a PZT plate similar to that used in the ^{67}Zn measurements. The absorber was made of enriched $K_4Fe(CN)_6\cdot3H_2O$ powder containing 0.8 mg/cm^2 of ^{57}Fe. The 14-keV γ radiation was detected with a 0.1-mm-thick NaI(Tl) scintillator[51] coupled to a low-noise photomultiplier tube[52] (PMT). The anode signal of the PMT was fed via a fast amplifier to a leading-edge discriminator. The time information of the arriving γ quantum was derived from the anode pulse produced by the first photoelectron. The output pulses of the discriminator were used as stop pulses of a time-to-amplitude converter. The start pulses were derived from the output of a function generator which produced the sinusoidal driving voltage. The time resolution of the measuring system was about 5 ns. Energy discrimination was made with ordinary slow pulse electronics by gating the analog-to-digital converter of the MCA.

V. EXPERIMENTAL RESULTS AND DISCUSSION

A. Calibration

Certain calibration measurements were performed during each measurement series. The low-frequency drive was calibrated by measuring the separation of the three innermost quadrupole lines of the ZnO spectrum. The width of the center line was determined from another spectrum measured with a maximum velocity of about twice the total experimental linewidth. An unfolded result of such an experiment is shown in Fig. 8. The distortion parameter in this measurement was $d\simeq0.02$, and

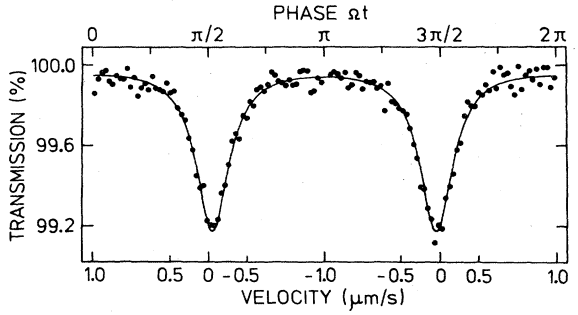

FIG. 8. Center line of a ^{67}Zn Mössbauer spectrum measured at a modulation frequency $f=\Omega/2\pi=130$ Hz. Data points are shown unfolded as a function of the phase Ωt of the sinusoidal Doppler modulation. Solid line is a least-squares fit by a Lorentzian curve. In the ^{67}Zn measurements the source was a ^{67}Ga:*ZnO* single crystal. In the case of Figs. 8—10, 11(a), and 13 the thickness of the enriched ^{67}ZnO-powder absorber was 1.29 g/cm^2.

thus an asymmetry of $\sim 2\%$ is expected from Eq. (3.4). The deviation from the Lorentzian (solid line) cannot be distinguished within the statistics. The fits of both the folded and unfolded data gave the same linewidth of 0.55(2) μm/s.

At frequencies considerably larger than the linewidth, the high-frequency transducer was calibrated by measuring the time average of the transmission intensity as a function of the driving voltage. The displacement amplitude $x_0=a\lambda$ is proportional to the amplitude of the sinusoidal voltage. An amplitude calibration at a phase-modulation frequency of 51.4 kHz is shown in Fig. 9. The amplitude was varied linearly with a period of about 10 s. As a first approximation the time average of the absorption is proportional to $J_0^2(a)$. The fit (solid line) includes also a correction due to the relatively low frequency of the phase modulation. In addition to the calibration this measurement gives information about the possible distribution of the displacement amplitude. Large amplitude distribution would produce a nonoscillating curve. At modulation frequencies close to the linewidth, TM measurements were used for the amplitude calibration (see below).

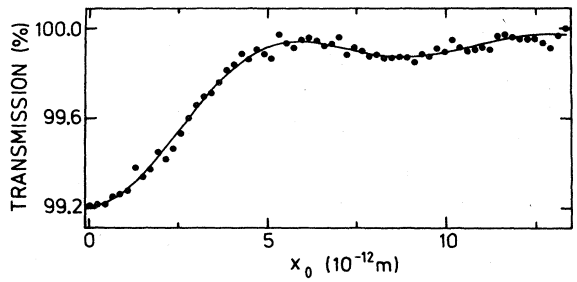

FIG. 9. Average transmission intensity as a function of the vibration amplitude x_0 of the source. Frequency of the sinusoidal modulation was 51.4 kHz. As a first approximation the absorption is proportional to $J_0^2(x_0/\lambda)$.

B. Sinusoidal modulation

Some results of TM measurements with sinusoidal phase modulation are presented in Fig. 10. The transmission curves have been obtained with approximately the same value of the modulation amplitude $a\simeq 11$. The data are shown unfolded as a function of the phase Ωt of the modulation. The solid curves are least-squares fits by Eq. (2.18) with $\varphi(t)$ given by Eq. (3.8). The dashed lines indicate the theoretical background intensity which would be observed in the absence of the Mössbauer resonance. This figure demonstrates how the time-dependent distortions of the Lorentzian transmission curves develop into coherent transients and further into quantum-beat oscillations.

The transmission curve of Fig. 10(a) was measured at a modulation frequency of 6 kHz and with a maximum velocity of 0.9 μm/s. As described in Sec. III A, the most evident deviations from the Lorentzian line shape are the delay, the asymmetry, and the line broadening (compare with Fig. 8). The transient oscillations are strongly damped due to the relatively low value of the distortion parameter ($d\simeq 0.9$). Figure 10(b) was obtained at a modulation frequency of 15 kHz with $d\simeq 6$. The damped interference oscillations are clearly visible. The absorber field contribution described by the third term in Eq. (3.7) enhances the first overshoot. Due to the overshoot the peak-to-peak effect is larger here than in conventional measurements. When the modulation frequency is still increased, only the quantum-beat oscillations remain. Figure 10(c) shows the result of a quantum-beat measurement, where the eighth and tenth harmonics of the modu-

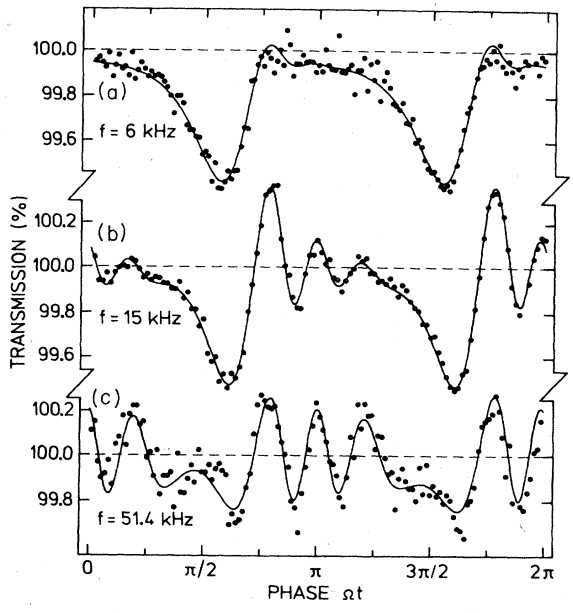

FIG. 10. Time dependence of the transmission intensity at modulation frequencies (a) $f<\Gamma_T/2\pi$, (b) $f\sim\Gamma_T/2\pi$, and (c) $f>\Gamma_T/2\pi$. Amplitude of the sinusoidal modulation was $x_0\simeq 2.3\times 10^{-11}$ m in all cases. Solid lines are least-squares fits by the theoretical expression (2.18).

lation frequency dominate in the transmission intensity. The frequency of the oscillations is largest near the velocity extrema at $\Omega t=\pi$ and 2π. By integrating the transmission curve it is seen that the average counting rate is about the same as it would be without the Mössbauer resonance. Such a situation occurs if the radiation entering the absorber is totally scattered in the forward direction.

The selection of the modulation amplitude and frequency deserves a comment in the case of Fig. 10(c). In this experiment the seventh harmonic of the modulation frequency was chosen to coincide with the quadrupole splitting in ZnO. The maximum velocity of the phase-modulation sweep was large enough to cover the nearest quadrupole lines. The effect of these lines on the time dependence was decreased by choosing the amplitude of the phase modulation close to a zero of J_7 as discussed in Sec. III A. A still larger modulation frequency (with $a\simeq 11$) would have also involved the next quadrupole line at -9.6 μm/s (see Fig. 6). The small deviation between the theoretical curve and the experimental data in Fig. 10(c) can be attributed to the residual distortion caused by the quadrupole line at $+4.8$ μm/s.

In Fig. 11, two transmission curves measured with the same modulation frequency (19.5 kHz) and amplitude ($a=6.3$) are shown. The measurements differ in the thicknesses of the absorbers, which were (a) 1.29 g/cm^2 and (b) 3.05 g/cm^2 of enriched ZnO. With the thicker absorber the first overshoot after the resonance is very pronounced because of the large contribution of the absorber field. The decay constants (linewidths) are (a) $2\Gamma_T\hat{=}0.59(3)$ μm/s and (b) $2\Gamma_T\hat{=}0.77(3)$ μm/s. Without background correction the observed peak-to-peak effects are 1.0% and 1.2%. The background corrected effects are 1.4% and 2.7%, respectively.

In Table I results from the least-squares fits of Figs. 10(b) and 11 are summarized. The statistical uncertainties of the fitted parameters are given in parentheses. Some additional data and results calculated from the fitted parameters are also shown. The data have been analyzed assuming that $\Gamma_a=1.25(25)\Gamma_0$, corresponding to 0.2 μm/s. The upper bound of Γ_a for this absorber material was obtained from the earlier linewidth data[10] after subtracting the line broadening caused by the absorber thickness and assuming that all the remaining broadening was due to the absorber only.

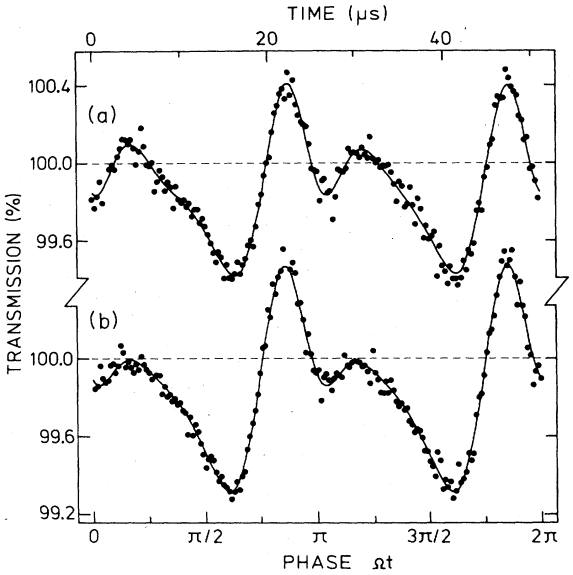

FIG. 11. Transmission curves obtained using sinusoidal modulation with $f=19.5$ kHz and $x_0=1.34\times10^{-11}$ m. Thicknesses of the two enriched ^{67}ZnO-powder absorbers were 1.29 g/cm^2 (a) and 3.05 g/cm^2 (b).

The displacement amplitude x_0 is calculated from the modulation amplitude a. The calibration of the amplitude of the mechanical motion is absolute in terms of the wavelength of the γ radiation. The resolution reached, 0.2 pm, is not easily achieved by other methods. The

TABLE I. Results from the least-squares fits by Eq. (2.18) to the data obtained with sinusoidal phase modulation. Measurements I, II, and III refer to Figs. 10(b), 11(a), and 11(b), respectively. Measurements I and II were performed with the same source and absorber.

Measurement	I	II	III
f (kHz)	15.0	19.5	19.5
D (g/cm^2)	1.29	1.29	3.05
Background correction	0.65(3)	0.72(3)	0.44(3)
Fitted parameters			
a	10.75(8)	6.36(7)	6.32(8)
$\Delta\omega$ (μm/s)	−0.040(3)	−0.042(5)	−0.016(3)
Γ_s (μm/s)	0.26(2)	0.27(2)	0.27(2)
f_s'	0.0139(16)	0.0144(20)	0.009 66(44)
T_a	2.58(34)	2.88(44)	7.60(56)
x_0 (pm)	22.7(2)	13.4(2)	13.4(2)
$2\Gamma_T$ (μm/s)	0.56(2)	0.59(3)	0.77(3)
f_s	0.0214(30)	0.0199(32)	0.0219(24)
f_a	0.0189(30)	0.0211(38)	0.0235(28)

voltage-to-displacement conversion factor of the quartz drive was obtained from measurement III, and it was later utilized in phase-switching experiments to adjust the phase shift $\Delta\varphi=\Delta x/\lambda$. The values of the center shift $\Delta\omega$ and the linewidth $2\Gamma_T$ are in agreement with the results obtained from conventional Mössbauer spectra.

The fit yields an uncorrected recoilless fraction of the source f_s'. The corrected recoilless fraction f_s is obtained by taking into account the background counts in the 93-keV energy window, an unresolved 91-keV line,[53] and pile-up of electronic pulses in the single-channel analyzer. The combined effect of these corrections is given in the table. The recoilless fraction of the absorber, f_a, is obtained from the Mössbauer thickness T_a by using Eq. (4.1). The weighted averages of the recoilless fractions are

$$f_s=0.0212(16),$$

$$f_a=0.0213(18).$$

The corresponding Debye temperatures of the source and absorber are $\Theta_D^s=316(6)$ K and $\Theta_D^a=316(7)$ K, respectively. Within the uncertainty, the recoilless fractions are equal. In light of the Debye model this is an expected result, when the very small shift between the source and absorber line positions is taken into account. An uncertainty of 2% was achieved in the Debye temperatures in spite of the fact that the measurement conditions were not optimal for the separation of the recoilless fractions (compare with Fig. 2). The outcome of these transient experiments is in agreement with the earlier result[54] $\Theta_D=309(10)$ K obtained assuming that $\Theta_D^s=\Theta_D^a$.

We finally present a result from transient experiments with ^{57}Fe and compare it with a ^{67}Zn measurement. In Fig. 12, unfolded center parts of transmission curves measured using these two resonances are shown. Figure 12(a) was obtained with sinusoidal phase modulation at a frequency of 1 kHz. Only the center line and the ensuing overshoot are presented, but the quadrupole lines of the spectrum were also seriously modified. The linewidth of the most often used Mössbauer isotope ^{57}Fe is considerably larger ($\Gamma_0/2\pi\simeq 1.1$ MHz) than that of ^{67}Zn. With ^{57}Fe the conditions for observing distorted line shapes are not normally fulfilled. Figure 12(b) presents a demonstration of transient effects with this isotope. The transmission curve was measured at a modulation frequency of 190 kHz. At this frequency the motion of the PZT drive used was slightly incoherent.

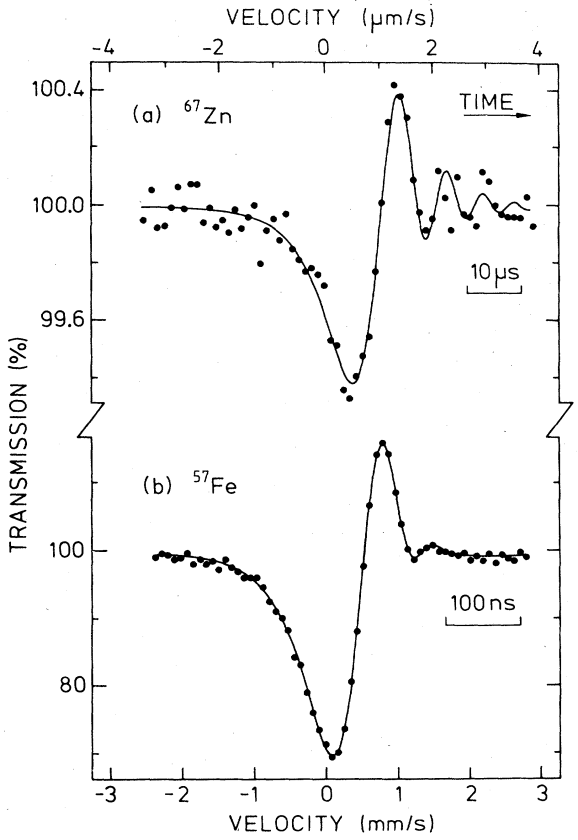

FIG. 12. Transmission curves measured with sinusoidal modulation using the Mössbauer resonances of ^{67}Zn and ^{57}Fe. Experimental parameters were (a) $f=1$ kHz, $v_{max}=15$ μm/s and (b) $f=190$ kHz, $v_{max}=9$ mm/s. Only the data near zero velocity are presented. Thickness of the enriched ^{67}ZnO-powder absorber was 1.6 g/cm^2. Curve (b) was obtained at room temperature with a ^{57}Co:*Rh* source and with an enriched $K_4Fe(CN)_6\cdot 3H_2O$ absorber containing 0.8 mg ^{57}Fe/cm^2.

C. Phase switching

We next discuss results obtained with periodic phase switching. As described in Sec. IV, the square-wave input voltage was filtered to avoid excitation of mechanical resonances. For illustration we first present a result of measurements *without filtering* (Fig. 13). The leading and trailing edges of the modulation are at 0 and 25 μs. The amplitude of the modulation corresponds to $\Delta\varphi\simeq\pi/2$. In accordance with the calculations of Sec. III B, the time dependence of the transmission intensity contains pronounced oscillations at the resonance frequency of the quartz drive. In addition to the oscillations there is a decaying background. It can be estimated that the amplitude of the vibration is $a_q\sim 1$, and that the voltage-to-displacement conversion factor at the resonance is about 50 times larger than that at low frequencies. Also, the

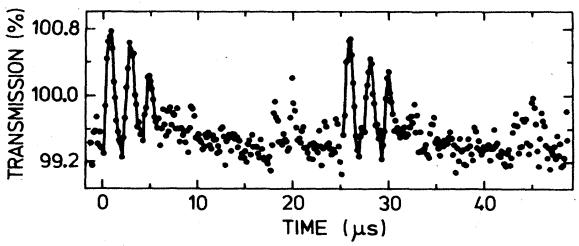

FIG. 13. Time dependence of the transmission intensity when a mechanical resonance of the drive is excited by phase switching. In contrast to Figs. 14 and 15 filtering of the driving voltage was *not* used here. Data points after the phase shifts at 0 and 25 μs are connected to clarify the resonance oscillations.

disturbances at ~ 20 and ~ 45 μs are probably related to the excitation of the mechanical resonances.

Results from measurements *with filtered* square-wave modulation are shown in Fig. 14. These data were obtained with a relatively thick absorber $T_a = 6.9(6)$. The solid lines are least-squares fits by Eq. (2.18) with $\varphi(t)$ functions shown in the upper part of Fig. 14. The transmission curve of Fig. 14(c) was measured with enhanced filtering of the frequency components near the mechanical resonances. The increased damping with $\Delta\varphi \simeq 3\pi$ was necessary because of the larger amplitude of the driving voltage as compared to the curves of Figs. 14(a) and 14(b). The time constants of the phase changes are 1 and 2 μs. Due to the band-reject filtering the actual driving voltage (with a and b) also included a small ($<5\%$) oscillating contribution associated with the changes of the phase.

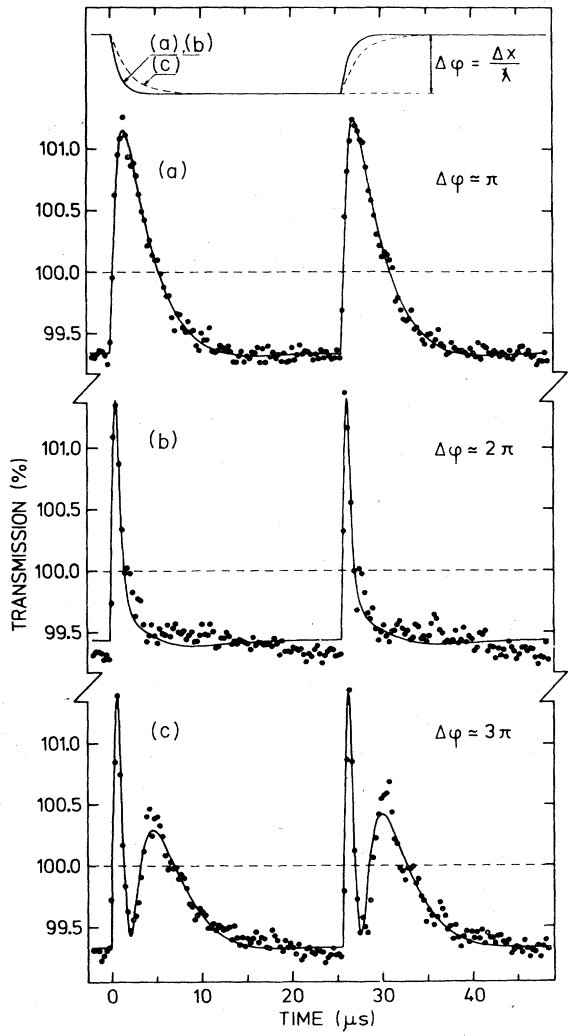

FIG. 14. Transmission curves obtained with phase shifts of (a) π, (b) 2π, and (c) 3π. Solid lines are least-squares fits by Eq. (2.18) with the phase modulation $\varphi(t)$ shown in the upper part of the figure. As the phase changes, the transmission intensity exceeds the background level indicated by the broken lines. Short γ-radiation pulses are observed during phase shifts of 2π. Thickness of the enriched ^{67}ZnO-powder absorber was 3.05 g/cm^2 here and in Fig. 15.

During the displacement the transmitted signal reaches a maximum which greatly exceeds the nonresonant background level indicated by the broken line. The measured effect, 2.1% peak-to-peak, is about 3 times as large as the conventional resonance absorption. With a modulation of zero rise time an intensity change of 2.6(2)% should have been observed according to Eq. (3.18). The reduction of the measured effect can be explained by decay of the transient during the phase shift. For this reason also the intensity change with $\Delta\varphi \simeq \pi$ is slightly smaller than with $\Delta\varphi \simeq 2\pi$. The background corrected effect is as large as 4.8%.

Rapid changes are observed in the time dependence of the transmission intensity in Fig. 14. The damping in Fig. 14(a) is not purely exponential but it exhibits a contribution of Bessel functions described by Eqs. (3.14) and (3.15). With $\Delta\varphi \simeq 2\pi$, short ($\sim 1$ μs) γ-radiation pulses are observed during the change of the phase. The transmission intensity first reaches a maximum, when the source has moved half a wavelength. Then, if the motion has stopped, the intensity decays back to the equilibrium value [Fig. 14(a)] or, if the motion continues, the intensity drops rapidly to the steady-state level after a displacement of another half-wavelength [Fig. 14(b)]. The transmission curve of Fig. 14(c) contains two γ pulses similar to those observed with $\Delta\varphi \simeq 2\pi$ and two damped responses of the phase shift $\Delta\varphi \simeq \pi$. The oscillatory behavior of the transmitted intensity can also be understood as an interference of the source and absorber radiation fields described by Eq. (3.20).

In the data of Fig. 14(b) there is a slow background drift in addition to the γ-radiation pulses. The drift is probably caused by residual excitation of the mechanical resonances of the drive. This contribution is not included in the fits and a visible deviation between the experimental and theoretical results exists. According to the considerations in Sec. III B, the background drift provides an estimate of the degree of disturbances remaining in spite of filtering of the driving voltage. Because the distortions are proportional to a_q^2, and a_q is proportional to $\Delta\varphi$, it can be expected that the background drift is negligible with $\Delta\varphi \simeq \pi$. This conclusion is supported by the good agreement between the experimental and theoretical curves of Fig. 14(a).

In the transmission curves of Fig. 14 the center shift is much smaller than the linewidth. New features in the transmission intensity appear when $\Delta\omega$ is increased. Figure 15 shows a result from phase-switching experiments with a considerably larger center shift $\Delta\omega \simeq 1.8\Gamma_0$. The center shift was intentionally produced with the low-frequency drive. The steady-state absorption was reduced by a factor of almost 2 as compared to the transmission curves of Fig. 14. The phase shift $\Delta\varphi \simeq \pi/2$ was chosen to maximize the effect of $\Delta\omega$ on the time dependence of the transmission intensity. The phase change at 25 μs corresponds to motion of the source towards the absorber. The transient beginning at 0 μs resembles those in Fig. 14(a), while the transient beginning at 25 μs is of opposite

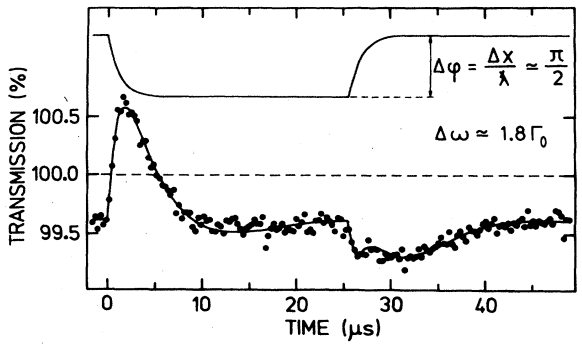

FIG. 15. Result of a phase-switching experiment with the center shift $\Delta\omega \hat{=} 0.29$ μm/s close to Γ_T. Because of the nonzero value of $\Delta\omega$, the two transients look very different. The phase shift $\Delta\varphi \simeq \pi/2$ was chosen to maximize the difference between the transients.

polarity. The transmission intensity stays quite a long period, ~ 7 μs, near the level determined by the maximum resonance absorption.

VI. SUMMARY

The coherent transient effects studied in this work resemble those observed in NMR and laser spectroscopy. In all these cases a resonance system is irradiated with highly monochromatic electromagnetic radiation. The main limitation of Mössbauer spectroscopy in regard to coherent transients is the low intensity of the source radiation, which does not allow observation of saturation effects. In Mössbauer experiments another type of saturation is achieved by using thick resonance absorbers. The absorber thickness can often be neglected in NMR and laser spectroscopy, but in Mössbauer spectroscopy it produces significant effects. Even with thick absorbers the simple model for the source radiation combined with the polarization described by Eq. (2.9) resulted in a good agreement between the theoretical calculations and the experimental data.

The transient effects are an important tool in basic research, and they can be utilized in several types of measurements. With sinusoidal phase modulation, the time dependence of the transmission intensity consists of an interference term and of another term depending mainly on the Mössbauer parameters of the absorbers. The latter term is more pronounced with thick resonance absorbers and it has a significant influence on the shape of the transmission curves only in transient experiments. Separation of the various contributions allows the determination of the recoilless fractions and linewidths of both the source and the absorber. These parameters are much less correlated in transient experiments than in conventional Mössbauer experiments. The interference oscillations can be used for accurate calibration of the phase modulation and, hence, of the mechanical displacement. The separation between the adjacent zeros of the interference oscillations corresponds to a displacement of the source by half a wavelength. In addition to calibration the oscillations give information about the possible phase incoherence of the modulation.

Large intensity changes were observed in phase-switching experiments. The background-corrected peak-to-peak effect of $\sim 4.8\%$ is more than 2 times the recoilless fraction of the source or of the absorber. The width of the γ-radiation pulses observed during phase changes of 2π can be controlled by varying the rise time of the modulation. However, it should be noted that at our counting rates only one modulation cycle of about 1000 actually produces a pulse containing a recoilless γ quantum.

Presently experimental difficulties, such as detector time resolution and incoherency of the phase modulation, limit the number of Mössbauer resonances which can be efficiently used in transient experiments. So far most transient measurements have been performed using the Mössbauer resonance of ^{67}Zn. However, ^{57}Fe should be a very favorable isotope for the transient studies in the near future. One should also be aware of the possible existence of the time-dependent effects when utilizing other Mössbauer isotopes with narrow lines.

ACKNOWLEDGMENTS

The authors thank Professor E. Byckling for his support of this work. We are indebted to Dr. J. Javanainen, Dr. W. Potzel, and Mr. M. Salkola for valuable discussions, and to Mr. T. Poikolainen from the Cyclotron Laboratory of the University of Jyväskylä for irradiation of the Mössbauer sources. The financial support of the Academy of Finland and the Finnish Cultural Foundation is gratefully acknowledged.

APPENDIX

The effect of line broadening on transient measurements is calculated in this Appendix. It is assumed that the broadening is caused by a distribution in the resonance frequencies of the source and absorber. We also derive a series expansion for the time dependence of the transmission intensity and discuss the extension of the theory to multiline sources and absorbers.

We consider first the energy spectrum of the source radiation. The Fourier-series expansion of the phase-modulation factor in Eq. (2.1) is

$$e^{i\varphi(t)} = \sum_{n=-\infty}^{\infty} C_n e^{in\Omega t} , \tag{A1}$$

where the coefficients are defined by an integral over the period of the modulation:

$$C_n = \frac{\Omega}{2\pi} \int_0^{2\pi/\Omega} e^{i[\varphi(t) - n\Omega t]} dt . \tag{A2}$$

The coefficients C_n are real if $\varphi(-t) = -\varphi(t)$. With sinusoidal modulation, $\varphi(t) = a \sin(\Omega t)$, they are Bessel functions, $C_n = J_n(a)$. Equation (A1) can be used to calculate the energy spectrum of the radiation described by the model of Eq. (2.1):

$$\int_{-\infty}^{\infty} dt_0 \, |E_s(x,\omega)|^2 \propto \sum_{n=-\infty}^{\infty} \frac{|C_n|^2}{(\omega-\omega_s-n\Omega)^2+(\Gamma_0/2)^2} , \tag{A3}$$

where $E_s(x,\omega)$ is the Fourier transform of $E_s(x,t)$. The spectrum consists of sidebands of width Γ_0 at angular frequencies $\omega=\omega_s+n\Omega$.

Broadening of the *source* line can be taken into account by replacing ω_s by $\omega_s+\eta$ in Eq. (A3) and choosing an appropriate distribution for the deviation η. When the integration over η is performed using a Lorentzian distribution

$$L(\eta)=\frac{\gamma}{2\pi}\frac{1}{\eta^2+(\gamma/2)^2} \tag{A4}$$

of width $\gamma=\Gamma_s-\Gamma_0$, the linewidth Γ_s is substituted for Γ_0 in Eq. (A3). The replacement of Γ_0 by Γ_s in Eq. (2.2) can be accomplished similarly. If a Gaussian distribution $G_s(\eta)$ is employed, the energy spectrum of the source radiation will consist of Voigt profiles.

By using a modification of Eq. (2.13),

$$a_g(\omega)=\exp\left[\int_{-\infty}^{\infty}\frac{ibG_a(\eta')d\eta'}{\omega-\omega_a-\eta'-i\Gamma_0/2}\right] , \tag{A5}$$

a distribution $G_a(\eta')$ in the resonance frequencies of the *absorber* can also be taken into account. The integration in Eq. (A5) corresponds to summing of the polarization contributions of the form of Eq. (2.9). The function $a_g(\omega)$ reduces to $a(\omega)$ when the integration is performed over the Lorentzian distribution (A4) with $\gamma=\Gamma_a-\Gamma_0$.

The explicit form of the distribution function depends on the case analyzed. In many cases a Gaussian distribution or an unresolved hyperfine splitting would be plausible choices. However, the Lorentzian approximation is more realistic when, e.g., broadenings due to dilute magnetic impurities are studied.[55] Since the calculations are considerably simpler with the Lorentzian distribution, this approximation is utilized in Secs. II and III.

We now turn to calculation of the transmission intensity. Equation (2.17) for the time dependence of the recoilless radiation can be written with the aid of the Fourier transforms

$$N'(t)\propto\int_{-\infty}^{\infty}dt_0\int_{-\infty}^{\infty}d\omega\int_{-\infty}^{\infty}d\omega' e^{it(\omega-\omega')}a(\omega)a^*(\omega') \times E_s(\omega)E_s^*(\omega') . \tag{A6}$$

Performing the t_0 integration first gives for the total intensity

$$N(t)=N_0\left[1-f_s+f_s\sum_{n,m=-\infty}^{\infty}C_nC_m^*e^{i(n-m)\Omega t}H_{nm}\right] , \tag{A7}$$

where

$$H_{nm}=\frac{\Gamma_s}{2\pi}\int_{-\infty}^{\infty}\frac{a(\omega+n\Omega)a^*(\omega+m\Omega)}{(\omega-\omega_s)^2+(\Gamma_s/2)^2}d\omega . \tag{A8}$$

The terms in Eq. (A7) can be readily interpreted as an interference between the nth and mth sidebands. A series expansion for H_{nm} can be found in Ref. 7, with a Lorentzian distribution of resonance frequencies in the source. Our treatment of the broadening of the absorber line is different from that presented in Ref. 7. Using general distribution functions, Eq. (A8) can be written as

$$H_{nm}^g=\frac{\Gamma_0}{2\pi}\int_{-\infty}^{\infty}d\omega\, a_g(\omega+n\Omega)a_g^*(\omega+m\Omega) \times\int_{-\infty}^{\infty}d\eta\frac{G_s(\eta)}{(\omega-\omega_s-\eta)^2+(\Gamma_0/2)^2} . \tag{A9}$$

When there is no modulation, only $C_0=1$ is nonzero, and the conventional transmission integral[36]

$$N(t)=N_0(1-f_s+f_sH_{00})=N_0\left[1-f_s+\frac{f_s\Gamma_s}{2\pi}\int_{-\infty}^{\infty}\frac{\exp\{-b\Gamma_a/[(\omega-\omega_a)^2+(\Gamma_a/2)^2]\}}{(\omega-\omega_s)^2+(\Gamma_s/2)^2}d\omega\right] \tag{A10}$$

with $b=T_a\Gamma_0/4$ results. Here T_a is the Mössbauer thickness of the absorber. In Eq. (A10), the angular frequency ω_s may include a slowly varying part due to Doppler modulation.

In the above derivation a single-line source and absorber were assumed. A generalization taking into account several lines in the source can be made by summing terms of the form of the right-hand side of Eq. (A7). With an absorber including several lines, summing of the individual lines should be performed in the exponent of the absorber response. In each term the thickness parameter b corresponds to the thickness of the line in question. A rigorous treatment of the multiline sources and absorbers would involve the polarization of the radiation.

*Present address: Weights and Measures Office, Technical Inspection Centre, P.O. Box 204, SF-00181 Helsinki 18, Finland.

[1]P. Helistö, T. Katila, W. Potzel, and K. Riski, Phys. Lett. **85A**, 177 (1981).

[2]P. Helistö, E. Ikonen, T. Katila, and K. Riski, Phys. Rev. Lett. **49**, 1209 (1982).

[3]T. Katila, P. Helistö, E. Ikonen, and K. Riski, in *Applications of the Mössbauer Effect* (Gordon and Breach, New York, in press), p. 213.

[4]K. Riski, P. Helistö, E. Ikonen, and T. Katila, Hyperfine Interact. **15/16**, 1021 (1983).

[5]R. Koch, E. Realo, K. Rebane, and J. Jógi, in Ref. 3.

[6]G. J. Perlow, Phys. Rev. Lett. **40**, 896 (1978).

[7]J. E. Monahan and G. J. Perlow, Phys. Rev. A **20**, 1499 (1979).

[8]G. L. Zhang, E. H. du Marchie van Voorthuysen, and H. de

Waard, Phys. Lett. **91A**, 417 (1982).
[9]E. H. du Marchie van Voorthuysen, G. L. Zhang, and H. de Waard, Phys. Rev. A **30**, 2356 (1984).
[10]P. Helistö, E. Ikonen, T. Katila, W. Potzel, and K. Riski, Phys. Rev. B **30**, 2345 (1984).
[11]N. Bloembergen, E. M. Purcell, and R. V. Pound, Phys. Rev. **73**, 679 (1948).
[12]B. A. Jacobsohn and R. K. Wangsness, Phys. Rev. **73**, 942 (1948).
[13]F. Bloch, Phys. Rev. **70**, 460 (1946).
[14]J. S. Gooden, Nature **165**, 1014 (1950).
[15]R. Gabillard, C. R. Acad. Sci. **232**, 1477 (1951); **232**, 1551 (1951).
[16]E. L. Hahn, Phys. Rev. **77**, 297 (1950).
[17]H. C. Torrey, Phys. Rev. **76**, 1059 (1949).
[18]E. L. Hahn, Phys. Rev. **80**, 580 (1950).
[19]R. P. Feynman, F. L. Vernon, and R. W. Hellwarth, J. Appl. Phys. **28**, 49 (1957).
[20]A. Z. Genack, D. A. Weitz, R. M. Macfarlane, R. M. Shelby, and A. Schenzle, Phys. Rev. Lett. **45**, 438 (1980).
[21]A. Z. Genack, R. O. Brickman, and A. Schenzle, Appl. Phys. B **28**, 276 (1982).
[22]A. Z. Genack, K. P. Leung, and A. Schenzle, Phys. Rev. A **28**, 308 (1983).
[23]R. G. Brewer and R. L. Shoemaker, Phys. Rev. A **6**, 2001 (1972).
[24]R. G. DeVoe and R. G. Brewer, Phys. Rev. Lett. **40**, 862 (1978).
[25]G. B. Hocker and C. L. Tang, Phys. Rev. Lett. **21**, 591 (1968).
[26]R. G. Brewer and R. L. Shoemaker, Phys. Rev. Lett. **27**, 631 (1971).
[27]N. A. Kurnit, I. D. Abella, and S. R. Hartmann, Phys. Rev. Lett. **13**, 567 (1964).
[28]B. E. A. Saleh, D. Stoler, and M. C. Teich, Phys. Rev. A **27**, 360 (1983).
[29]W. E. Lamb, Phys. Rev. **134**, A1429 (1964).
[30]F. A. Hopf, R. F. Shea, and M. O. Scully, Phys. Rev. A **7**, 2105 (1973).
[31]R. G. Brewer, in *Frontiers in Laser Spectroscopy,* edited by R. Balian, S. Haroche, and S. Liberman (North-Holland, Amsterdam, 1977), Vol. 1, p. 342.
[32]Yu. Kagan, A. M. Afanas'ev, and V. G. Kohn, J. Phys. C **12**, 615 (1979).
[33]F. J. Lynch, R. E. Holland, and M. Hamermesh, Phys. Rev. **120**, 513 (1960).
[34]S. M. Harris, Phys. Rev. **124**, 1178 (1961).
[35]M. K. F. Wong, Proc. Phys. Soc. London **85**, 723 (1965).
[36]D. A. O'Connor, Nucl. Instrum. Methods **21**, 318 (1963).
[37]*Handbook of Mathematical Functions,* edited by M. Abramowitz and I. A. Stegun (Dover, New York, 1970), p. 300.
[38]I. S. Gradshteyn and I. M. Ryzhik, *Table of Integrals, Series, and Products* (Academic, New York, 1973), p. 710.
[39]Atomergic Chemetals Corp., New York, U.S.A.
[40]Techsnabexport, Moscow, U.S.S.R.
[41]T. Katila, A. Niemi, K. Riski, and J. Ylä-Jääski, Helsinki University of Technology Report No. TKK-F-A400, 1979 (unpublished).
[42]G. J. Perlow, W. Potzel, R. M. Kash, and H. de Waard, J. Phys. (Paris) Colloq. **35**, C6-197 (1974).
[43]W. Potzel, T. Obenhuber, A. Forster, and G. M. Kalvius, Hyperfine Interact. **12**, 135 (1982).
[44]*Mössbauer Effect Data Index 1976,* edited by J. G. Stevens and V. E. Stevens (Plenum, New York, 1978), p. 171.
[45]M. T. Hirvonen, T. Katila, K. Riski, and J. Tanttu, Phys. Rev. B **24**, 11 (1981).
[46]P. Helistö, Helsinki University of Technology Report No. TKK-F-A563, 1985 (unpublished).
[47]Vernitron Ltd., Southampton, England.
[48]Valpey-Fisher Corp., Hopkinton, MA, U.S.A.
[49]D. Griesinger, R. V. Pound, and W. Vetterling, Phys. Rev. B **15**, 3291 (1977).
[50]E. Ikonen, P. Karp, T. Katila, and K. Riski, J. Phys. E **16**, 875 (1983).
[51]Harshaw Chemie B. V., De Meern, Holland.
[52]Hamamatsu 2060 PMT, Hamamatsu, Japan.
[53]R. A. Meyer, A. L. Prindle, W. A. Myers, P. K. Hopke, D. Dieterly, and J. E. Koops, Phys. Rev. C **17**, 1822 (1978).
[54]W. Potzel, A. Forster, and G. M. Kalvius, J. Phys. (Paris) Colloq. **37**, C6-691 (1976).
[55]A. Abragam, *The Principles of Nuclear Magnetism* (Oxford University, Oxford, 1961), p. 125.